Article

Synthesis and Catalytic Features of Hybrid Metal Nanoparticles Supported on Cellulose Nanofibers

Akihiro Azetsu [1], Hirotaka Koga [2,*], Akira Isogai [2] and Takuya Kitaoka [1,3,*]

[1] Department of Agro-Environmental Sciences, Graduate School of Bioresource and Bioenvironmental Sciences, Kyushu University, 6-10-1 Hakozaki, Higashi-ku, Fukuoka 812-8581, Japan; E-Mail: a-azetsu@agr.kyushu-u.ac.jp

[2] Department of Biomaterials Sciences, Graduate School of Agricultural and Life Sciences, The University of Tokyo, 1-1-1 Yayoi, Bunkyo-ku, Tokyo 113-8657, Japan; E-Mail: aisogai@mail.ecc.u-tokyo.ac.jp

[3] Biotron Application Center, Kyushu University, 6-10-1 Hakozaki, Higashi-ku, Fukuoka 812-8581, Japan

* Authors to whom correspondence should be addressed;
  E-Mails: ahkoga@mail.ecc.u-tokyo.ac.jp (H.K.); tkitaoka@agr.kyushu-u.ac.jp (T.K.).

Abstract: The structural and functional design of metal nanoparticles has recently allowed remarkable progress in the development of high-performance catalysts. Gold nanoparticles (AuNPs) are among the most innovative catalysts, despite bulk Au metal being regarded as stable and inactive. The hybridization of metal NPs has attracted major interest in the field of advanced nanocatalysts, due to electro-mediated ligand effects. In practical terms, metal NPs need to be supported on a suitable matrix to avoid any undesirable aggregation; many researchers have reported the potential of polymer-supported AuNPs. However, the use of conventional polymer matrices make it difficult to take full advantage of the inherent properties of the metal NPs, since most of active NPs are imbedded inside the polymer support. This results in poor accessibility for the reactants. Herein, we report the topochemical synthesis of Au and palladium (Pd) bimetallic NPs over the surfaces of 2,2,6,6-tetramethylpiperidine-1-oxyl (TEMPO)-oxidized cellulose nanofibers (TOCNs), and their exceptional catalytic performance. Highly-dispersed AuPdNPs were successfully synthesized *in situ* on the crystal surfaces of TOCNs with a very high density of carboxylate groups. The AuPdNPs@TOCN nanocomposites exhibit excellent catalytic

efficiencies in the aqueous reduction of 4-nitrophenol to 4-aminophenol, depending on the molar ratios of Au and Pd.

Keywords: gold; palladium; bimetallic nanoparticles; cellulose nanofiber; catalytic reduction; ligand effect; topochemical synthesis

---

1. Introduction

Metal nanoparticles have a variety of attractive properties, which enable them to play significant roles in a broad range of electronic, optical, biochemical and catalytic applications [1–4]. Gold nanoparticles (AuNPs) have become a central topic of academic and industrial interest as a promising candidate for next-generation nanocatalysts, even though bulk Au is stable and chemically inert [5–7]. Furthermore, in recent decades bimetallic NPs have also attracted attention for their specific characteristics being much different from those of the monometallic individuals [8–11]. The electronic interactions between two metal NPs are known to accelerate catalytic reactions. These so-called ligand effects result in a higher process efficiency compared to the monometallic equivalent. It has been reported that bimetallic NPs, comprising Au and palladium (Pd) have a higher catalytic activity towards the oxidation of alcohols in an aqueous solution than the individual monometallic NPs [12]. Similarly, Au–Ag and Au–Ni bimetallic NPs exhibit higher catalytic activities towards CO oxidation reactions [13] and the hydrolysis of ammonia borane [14], respectively, in comparison to the monometallic equivalents. Therefore, the hybridization of two different metal NPs is of great importance in the structural and electrochemical design of catalysts.

However, metal NPs are generally unstable due to their large active surface areas, so preventing their self-aggregation, which causes a huge drop in a catalytic activity, is critical for practical use. Surface coating with surfactants and/or various chemical modifications of the metal NPs have been carried out to stabilize them and maintain the original size dispersions [15–17]. Another effective approach to inhibit aggregation is to immobilize the metal NPs on various matrices, such as metal oxides or polymers [18–20]. In fact, polymer-NPs nanocomposites are attracting attention for practical applications; their mechanical and catalytic properties have been extensively investigated. Polymer-type matrices with thiol, pyridyl, amine and carboxyl groups as anchor sites for the metal NPs are highly tunable for further improvement. However, polymer matrices have the following disadvantages for catalyst immobilization: (1) poorly regulated anchor sites; (2) low thermal stability; and (3) the embedding of active metal NPs inside the polymer layers [21–23]. Therefore, to achieve high catalytic performances, the structural and functional design of catalyst supports for metal NPs is required for the regulated immobilization of exposed active metal NPs on the outer surfaces of thermally-stable matrices. Furthermore, many polymer matrices are made from non-renewable petrochemicals, so alternative, environmentally-friendly polymer supports are required.

Cellulose is the most abundant natural polymer, originating from plants, tunicates and bacteria [24–26]. Native cellulose consists of nanometer-sized fibrils, 3–20 nm in width, and has an extremely high crystallinity up to 65–95%, depending on their origin [27–32]. Since cellulose nanofibrils strongly bind to each other through hydrogen bonding, it is very difficult to obtain individual cellulose nanofibers.

Mechanical and/or acid treatments have been studied to prepare dispersed nanofibers. However, only bundles of cellulose nanofibril fractions were obtained, which in some cases led to drastic decreases in both yield and fiber length [33–39].

Recently, it has been reported that 2,2,6,6-tetramethylpiperidine-1-oxyl (TEMPO) catalyzes the selective oxidation of the C6 primary hydroxyl group of cellulose to a carboxylate, which is only present on the surfaces of each crystalline cellulose nanofibril under mild aqueous conditions [40]. This TEMPO-mediated oxidation can provide a new type of natural polymer assembly, *i.e.*, individually-dispersed crystalline cellulose nanofibers with a high carboxylate density. These accumulate exclusively on their surfaces and act as anchor sites for metal NPs synthesis. The TEMPO-oxidized cellulose nanofibers (TOCNs) have unique physicochemical properties, such as high crystallinity (up to 95%), high stiffness (1.38 GPa), a low thermal–expansion coefficient (0.1 ppm K^{-1}), high density (1600 kg m^{-3}) and very high surface carboxylate densities up to 1.52 mmol g^{-1} (theoretical charge: 0.6 C m^{-2}) [41–44]. Therefore, TOCNs are recognized for their suitability as matrices for metal NPs-shaped catalysts and their potential to overcome the disadvantages of polymer-type matrices. In our previous trial, AuNPs were successfully synthesized on TOCNs from tunicates, and the characteristic AuNPs exposed on the surface of the TOCNs made great contribution to the high catalytic performances observed [45].

In the present study, we report the topochemical synthesis of AuPd-bimetallic NPs on TOCNs obtained from softwood cellulose, by exploiting the unique morphological and chemical properties of wood TOCNs. Highly-dispersed AuNPs, PdNPs and hybrid AuPdNPs form in high-density after selective reaction with the carboxylate groups on the TOCN surfaces. The obtained nanocomposites, AuNPs@TOCN, PdNPs@TOCN and AuPdNPs@TOCN, were compared in terms of catalytic behavior in the model reduction of 4-nitrophenol (4-NP) to 4-aminophenol (4-AP) in an aqueous medium. The molar ratios of Au and Pd in the hybrid NPs@TOCN are investigated for the enhancement of catalytic efficiency, based on the ligand effects between the Au and Pd components.

2. Results and Discussion

2.1. Structural Characteristics of Metal NPs@TOCN Nanocomposites

The topochemical syntheses of AuNPs, PdNPs and AuPd bimetallic NPs were carried out on a TOCN support in an aqueous sodium borohydride ($NaBH_4$) system. The TOCN surface possessed a high-density of carboxyl groups (0.96 mmol g^{-1}) on the crystalline surfaces, which serve as anchor sites for metal NPs synthesis. Figure 1 shows the UV-vis absorption spectra for the AuNPs with and without TOCN. In both cases, clear surface plasmon resonance (SPR) bands at around 520 nm are observed. The SPR absorption occurs on the boundary surface of AuNPs having free electrons in the conduction band due to coherent vibrational oscillation of the surface free electrons induced by incident light of visible wavelength region. The mixture of TOCN and tetrachloroaurate ($HAuCl_4$) aq. immediately changed from colorless to reddish pink upon the addition $NaBH_4$ aq., suggesting the successful formation of AuNPs [46]. The characteristic color depends upon the size and the shape of the particles; the AuNPs@TOCN composite showed a narrow SPR band at 508 nm, indicating the

formation of small size of AuNPs. Conversely, TOCN-free AuNPs have a broad band shifted to longer wavelength, suggesting the aggregation of AuNPs [47].

Figure 1. UV-vis absorption spectra of AuNPs in the presence (**a**) and absence (**b**) of TOCNs.
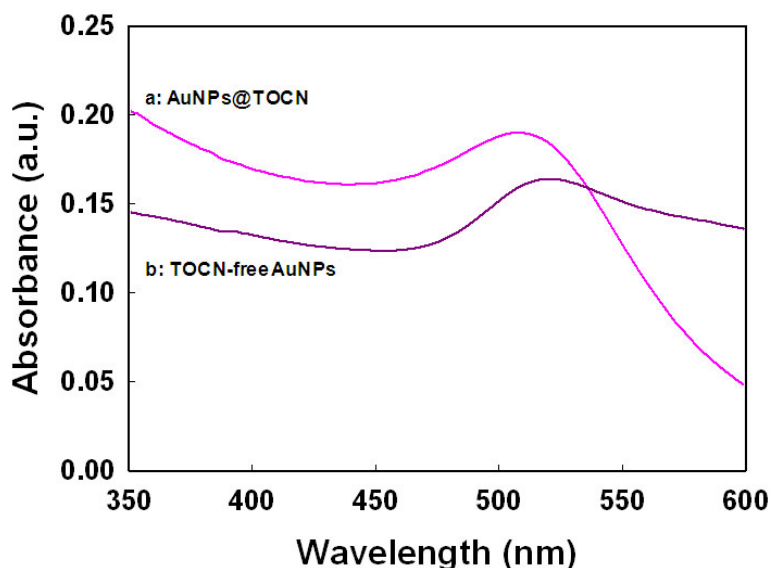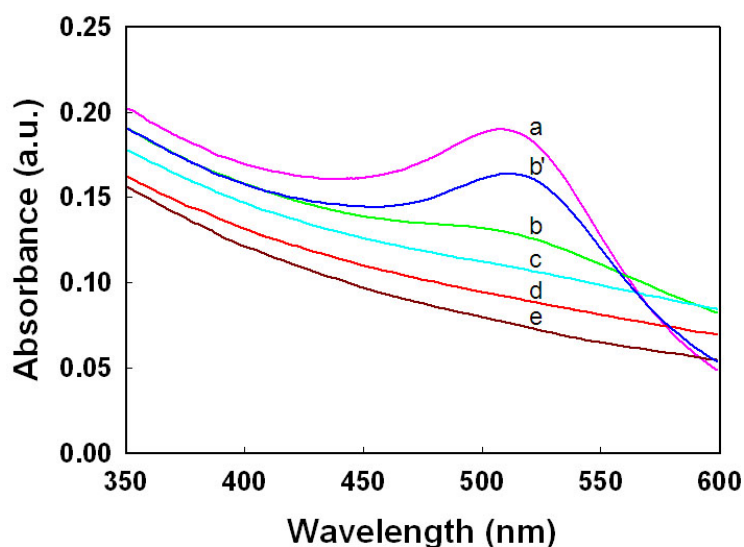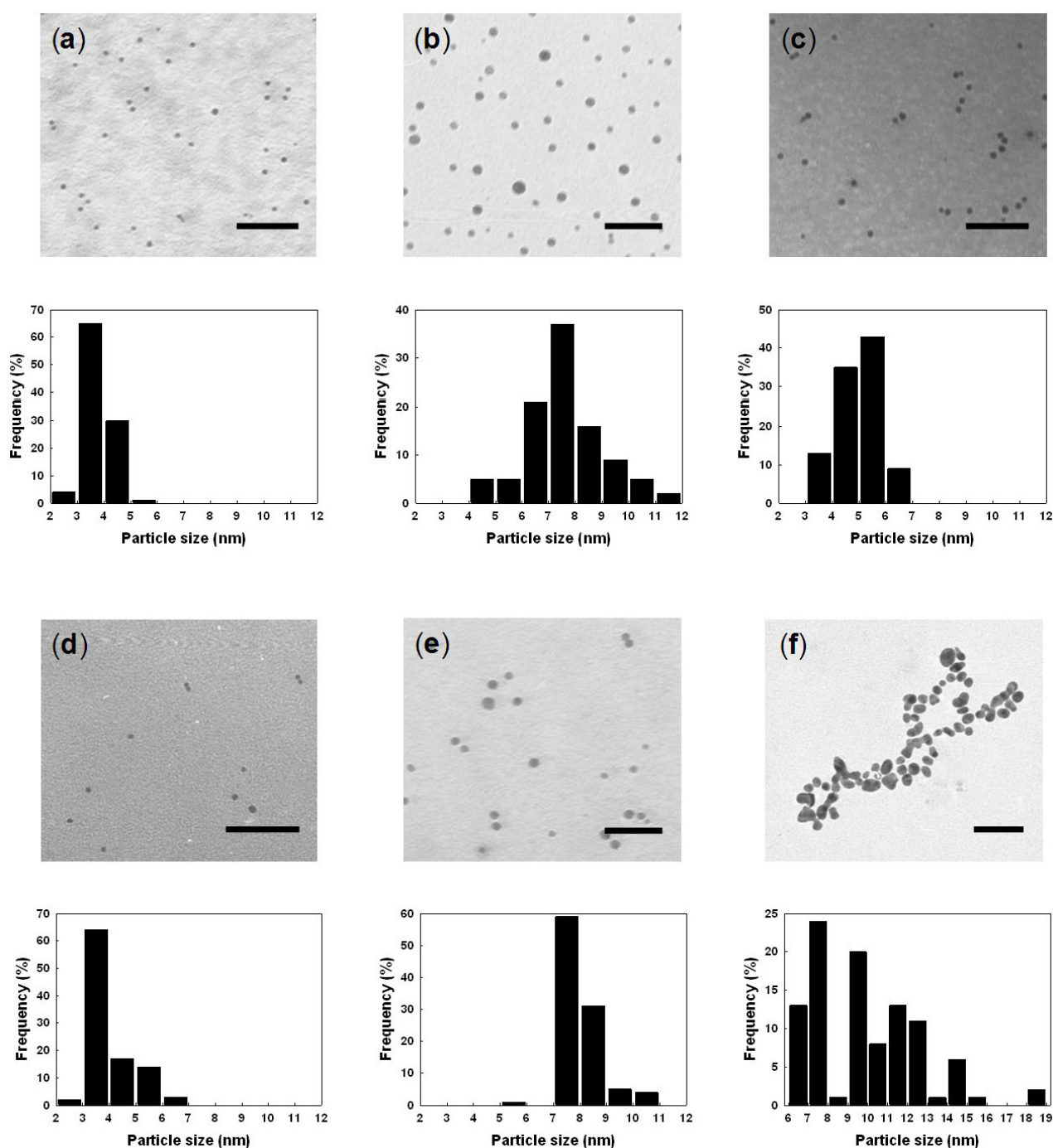

Figure 2 shows the UV-vis spectra for AuPdNPs[@]TOCN composites with various molar ratios of Au and Pd, and PdNPs[@]TOCN. The characteristic SPR bands rapidly disappeared upon increasing the Pd component. Physically-mixed suspensions of AuNPs[@]TOCN and PdNPs[@]TOCN, with a molar ratio of 3:1 for Au:Pd, displayed an obvious AuNPs[@]TOCN SPR band. The hybrid metal NPs[@]TOCN, prepared by mixing Au and Pd ions with a molar ratio of 3:1 in the synthesis, exhibited no significant SPR band. These results may indicate that the Au and Pd components in hybrid metal NPs[@]TOCN composites interact with each other electronically [48].

Figure 2. UV-vis absorption spectra for various metal NPs[@]TOCN composites with molar ratios of Au:Pd = (**a**) 1:0; (**b**) 3:1; (**c**) 1:1; (**d**) 1:3 and (**e**) 0:1; (**b'**) a physical mixture of AuNPs[@]TOCN and PdNPs[@]TOCN with a molar ratio of Au:Pd = 3:1.

The TEM images and size distribution histograms for the metallic NPs of AuNPs@TOCN, PdNPs@TOCN, AuPdNPs@TOCN and TOCN-free AuNPs are illustrated in Figure 3. Both the monometallic and bimetallic NPs were well dispersed in the presence of TOCN supports. The average particle sizes for the AuNPs@TOCN and PdNPs@TOCN composites were 4.01 ± 0.69 and 8.21 ± 0.86 nm, respectively, indicating a smaller size for the AuNPs on the TOCN supports. AuPdNPs on the TOCN supports, with Au:Pd molar ratios of 3:1, 1:1 and 1:3, had particle sizes of 7.70 ± 1.49, 5.18 ± 0.67 and 4.27 ± 0.85 nm, respectively.

Figure 3. TEM images and size distribution histograms for various metal NPs@TOCN composites, with molar ratios of Au:Pd = (**a**) 1:0; (**b**) 3:1; (**c**) 1:1; (**d**) 1:3; (**e**) 0:1 and (**f**) TOCN-free AuNPs. Scale bars correspond to 50 nm.

The TOCNs were invisible in the TEM images since no staining with heavy metals such as osmium, lead, uranium or gold was applied to clearly recognize metal NPs on the TOCN supports. The AuNPs without TOCN are significantly larger (9.93 ± 2.66 nm) than those in AuNPs@TOCN, and large distributions were also observed. This may reflect partial aggregation, as shown in Figure 3(f). Thus, strong interactions between the metal precursor cations and the dissociated carboxyl groups on the crystalline surface of TOCNs make a contribution to the uniform and tight immobilization of the metal NPs on the TOCN supports.

Figure 4 displays the HRTEM image of the nano-sized NPs of AuPdNPs@TOCN (Au:Pd = 3:1) and the corresponding EDX spectrum. The electron density and the lattice spacing of one metal NP were differently observed, depending on the position; however the detailed identification was difficult. The EDX profile of the single metal NP indicates the existence of both Au and Pd components in one NP. Therefore, Au and Pd nanocomponents are in contact to form one NP [49]. Figure 5 illustrates the AFM image for AuPdNPs@TOCN (Au:Pd = 3:1), and shows the surface morphology at a nanometer level. The height data of fibrous and granular matters were 1.8 ± 0.3 and 6.7 ± 0.7 nm, respectively, being in approximate agreement with the estimated ones of TOCN and AuPdNPs, although a certain degree of dry compression was found in the tapping-mode AFM analysis under ambient conditions. These particles may be metal NPs present on the surfaces of crystalline softwood TOCN; exposed, nano-dispersed metal NPs on the TOCN support were expected to enhance the catalytic activities.

Figure 4. EDX spectrum and HRTEM (inset) for the AuPdNPs@TOCN composite, with a molar ratio of Au:Pd = 3:1. Scale bar corresponds to 2 nm.
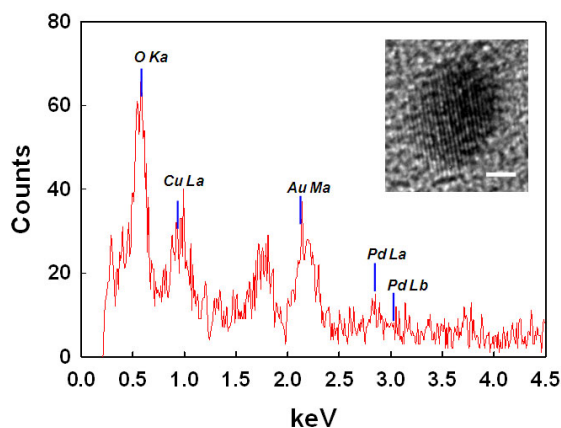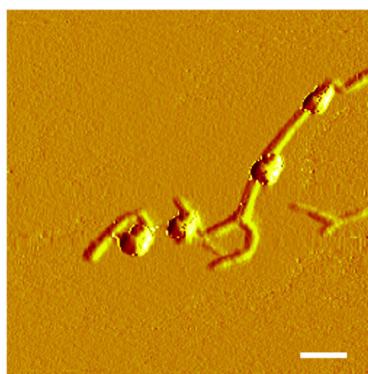

Figure 5. AFM image for the AuPdNPs@TOCN composite (Au:Pd = 3:1). Scale bar corresponds to 100 nm. *Notice: horizontal resolution is limited in analytical principle.*

2.2. Catalytic Performance of Hybrid Metal NPs@TOCN Composites

The catalytic efficiency of the as-designed metal NPs@TOCNs for the reduction of 4-NP to 4-AP was tested in the presence of $NaBH_4$. According to the literature protocol, the catalytic reduction rate is regarded as independent of the concentration of $NaBH_4$ [50]. Upon adding $NaBH_4$ to the 4-NP solution, the color of the solution changes from light yellow to dark yellow due to 4-nitrophenolate ion formation. The reaction progress was monitored using UV-vis spectrometry. Figure 6 shows the time-lapse UV-vis absorption spectra recorded throughout the catalytic reaction of 4-NP over AuNPs@TOCN. The yellow color of the 4-nitrophenolate ion faded with time after the addition of AuNPs@TOCN. The characteristic peak for 4-NP at 400 nm, assigned to the 4-nitrophenolate ion, gradually decreases; while a new peak at 300 nm, corresponding to 4-AP appears. The reaction was complete within 24 min at 25 °C. When TOCN-free AuNPs were used in the presence of $NaBH_4$, a negligible change detected, indicating that the aggregated AuNPs, as shown in Figure 3(f), have a poor catalytic activity. Figure 7 shows a linear correlation between $\ln(A_t/A_0)$ and reaction time at 25 °C, where A_t is the absorbance at the designated time and A_0 is the initial absorbance at t = 0. These results indicate that the catalytic reduction proceeds with pseudo-first-order behavior. The pseudo-first-order rate constant k at 25 °C for AuNPs@TOCN, as calculated from the slope, was 2.6×10^{-3} s^{-1}, while that for the TOCN-free AuNPs was 1.0×10^{-4} s^{-1}. Therefore, the TOCN serves as a very effective catalyst support, and the exposed AuNPs dispersed over the crystalline surface of TOCN, as shown in Figure 5, make a great contribution to the improved catalytic efficiency. Table 1 compares the turnover frequency (TOF) values for various polymer-supported AuNPs and AuNPs@TOCN designed in this study. The AuNPs@TOCN exhibits a significantly higher catalytic performance, ranging from 3 to *ca*. 1000 times higher, than those observed with conventional polymer-supported AuNPs. The as-reported polymer micelles, hydrogels and capsules inevitably distribute metal NPs inside the polymer layers, resulting in poor accessibility for the reactants to the active surfaces of metal NPs. Conversely, in the case of TOCN, active AuNPs are highly dispersed and exposed on the outer surface of the TOCN support, which enables an effective contact with the reactants. Therefore, AuNPs@TOCN may demonstrate a much higher catalytic activity than conventional AuNPs-containing polymer matrices.

Figure 6. UV-vis absorption spectra variations throughout the catalytic reduction of 4-NP over AuNPs@TOCNs.
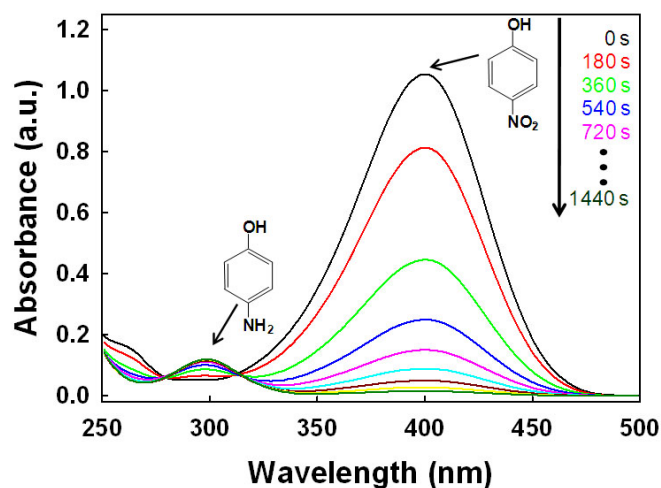
Figure 7. $\ln(A_t/A_0)$ *versus* reaction time for the catalytic reduction of 4-NP; AuNPs@TOCN (squares) and TOCN-free AuNPs (triangles).
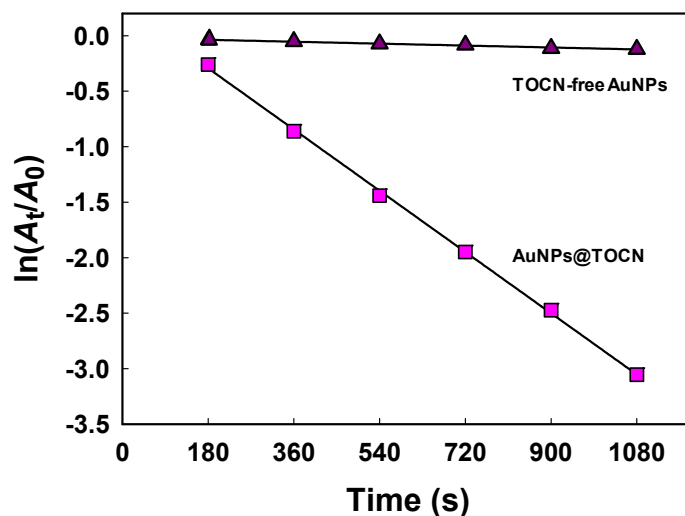

Table 1. Recent studies on the catalytic reduction efficiency of 4-NP over Au nanocatalysts.

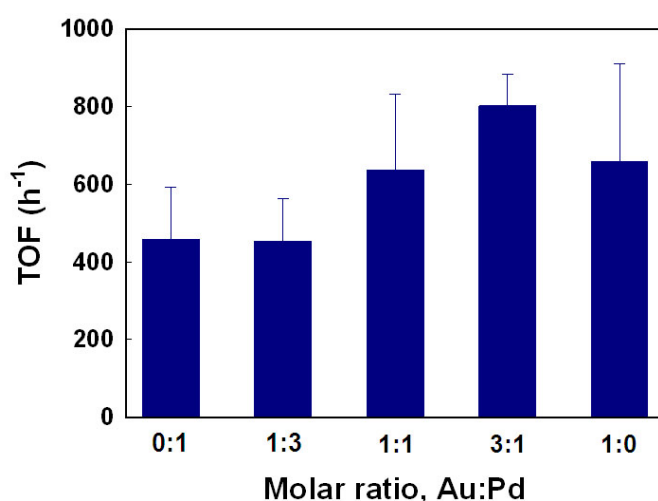| Entry	Supporting material	Au size [a] (nm)	T [b] (K)	NaBH$_4$/4-NP/Au (mol/mol/mol)	k per Au content [c] (s^{-1} μmol-Au^{-1})	TOF [d] (h^{-1})	Ref.
1	PNIPAM-*b*-P4VP [e]	3.3	298	167/5/1	2.5×10^{-2}	15.5	[22]
2	PMMA [f]	6.9	295	22,500/15/1	9.0×10^{-2}	88.6	[50]
3	PDMAEMA-PS [g]	4.2	298	28/0.14/1	2.3×10^{-3}	0.673	[51]
4	Poly(DVB-*co*-AA) [h]	10	298	9800/267/1	4.1×10^{-2}	222	[52]
5	Chitosan [i]	3.1	303	20/6/1	5.0×10^{-3}	50.4	[53]
6	α-CD [j]	20	298	250/6/1	7.8×10^{-2}	34.0	[54]
7	TOCN	4.0	298	36,000/180/1	1.3×10^{-1}	657	This work

[*a*] Average diameter determined by TEM; [*b*] Reaction temperature; [*c*] Pseudo-first-order reaction rate constant per total Au content; [*d*] Turnover frequency values, which were estimated from the data given in the corresponding references; [*e*] Poly(*N*-isopropylacrylamide)-*block*-poly(4-vinylpyridine); [*f*] Poly(methyl methacrylate); [*g*] Poly(2-(dimethylamino)ethyl methacrylate)-grafted onto solid polystyrene core; [*h*] Poly(divinylbenzene-*co*-acrylic acid); [*i*] Chitosan-coated iron oxide; [*j*] α-Cyclodextrin.

2.3. Hybrid Effect of AuPdNPs@TOCN Composites on Catalytic Efficiency

The catalytic behaviors of AuNPs@TOCN, PdNPs@TOCN and AuPdNPs@TOCN were investigated in detail. The pseudo-first-order rate constant for PdNPs@TOCNs was 1.5×10^{-3} s^{-1}, lower than that for AuNPs@TOCN (2.6×10^{-3} s^{-1}). Thus, PdNPs were inferior to AuNPs in the catalytic reduction of 4-NP. However, interesting phenomena were observed with regard to AuPdNPs@TOCNs, with molar ratios of 3:1, 1:1 and 1:3 for Au:Pd; pseudo-first-order rate constants were 4.8×10^{-3}, 2.8×10^{-3} and 1.3×10^{-3} s^{-1}, respectively. Therefore, AuPdNPs@TOCN with a 3:1 of Au:Pd, demonstrates the highest catalytic efficiency of all the as-designed nanocomposites. Figure 8 shows the TOF values for AuNPs@TOCN, PdNPs@TOCN and AuPdNPs@TOCN. The AuPdNPs@TOCN with a 3:1 ratio of Au:Pd exhibited the highest TOF value, which reached 800 h^{-1}. These unique features may be attributed to ligand effects [12]. The proposed mechanism for the 4-NP reduction is as follows: (1) the adsorption of 4-nitrophenolate to the metal NP surfaces, which is the rate-determining step; (2) hydride

transfer from the metal NPs (especially AuNPs) to the 4-nitrophenolate; and (3) the reduction of 4-NP to 4-AP [55]. Au is more electronegative than Pd, and thus some electronic polarization must occur at the interface between Au and Pd, which results in a favorable interaction between PdNPs and the 4-nitrophenolate species. This can accelerate the rate-determining step [56]. Such electronic ligand effects presumably enhance the apparent catalytic activity and efficiency for the 4-NP reduction. A one-pot, simultaneous reduction of Au and Pd precursor ions, in the presence of TOCN was effective for the structural and functional design of hybrid metal NPs, immobilized and exposed on TOCN supports.

Figure 8. Turnover frequencies for the catalytic reduction of 4-NP over metal NPs$^{@}$TOCN composites, with various molar ratios of Au and Pd.

3. Experimental Section

3.1. Materials

Tetrachloroaurate hydrate (HAuCl$_4$·3H$_2$O) was purchased from TANAKA Kikinzoku Kogyo, Co. Ltd., Tokyo, Japan. Tetraamminepalladium (II) chloride ([Pd(NH$_3$)$_4$]·Cl$_2$) and sodium borohydride (NaBH$_4$) were obtained from Wako Chemical Industry, Co. Ltd., Osaka, Japan. TOCN suspensions (1.0 wt%, COOH-0.96 mmol g^{-1}) were provided by Nippon Paper Industries, Co. Ltd., Tokyo, Japan. The water used in this study was purified with a Milli-Q system (Millipore, Co. Ltd., Tokyo, Japan). Other chemicals were of reagent grade and used without further purification.

3.2. Preparation of Metal NPs$^{@}$TOCN Composites

Metallic NPs were synthesized in the presence of a TOCN suspension with varying molar ratios of Au:Pd (1:0, 3:1, 1:1, 1:3 and 0:1). An aqueous solution of HAuCl$_4$·3H$_2$O (0.20 mM, 1.5 mL) and [Pd(NH$_3$)$_4$]·Cl$_2$ (0.20 mM, 0.5 mL) was added to an aqueous suspension of TOCN (0.20 wt%, 2 mL) for a 3:1 Au:Pd bimetallic system. The total volumes of the Au and Pd solutions were kept to 2.0 mL, and the molar ratios were controlled by varying volume ratios. The mixture was stirred at 4 °C for 30 min, followed by the drop wise addition of NaBH$_4$ (6 mM, 2 mL). The reaction mixture was kept at

4 °C for 90 min with stirring, and the metal NPs@TOCN composites were synthesized by reduction of the metal ion precursors. As a control, TOCN-free AuNPs were similarly synthesized without TOCN.

3.3. Characterization

UV-vis spectra were recorded using a UV-visible spectrophotometer (Hitachi, Ltd., Tokyo, Japan) with a scan range of 250–600 nm and an optical path length of 10 mm. Transmission electron microscopy (TEM) was performed using a JEM1010 instrument (JEOL, Ltd., Tokyo, Japan) at 80 kV. For TEM analysis, one drop (*ca.* 10 µL) of the metal NPs@TOCN suspension was gently placed on a carbon-coated Cu grid, hydrophilized via plasma discharge, and dried at room temperature. High-resolution TEM (HRTEM) and energy dispersive X-ray spectrometry (EDS) images were obtained using a JEM2010 (JEOL, Ltd., Tokyo, Japan) at 200 kV. Atomic force microscopy (AFM) was performed under ambient conditions using a NanoScope IIIa AFM apparatus (Veeco Instrument, Inc., Plainview, NY, USA) in tapping mode. One drop (*ca.* 30 µL) of diluted metal NPs@TOCN suspension was gently placed on mica, and then dried at room temperature for AFM imaging.

3.4. Catalytic Performance Test

The catalytic reduction of 4-NP (0.06 mM, 60 mL) was measured at 25 °C in the presence of NaBH$_4$ (0.72 mmol) as a hydrogen source. An aqueous dispersion of metal NPs-TOCN composite (300 µL, total metal content: 0.02 µmol) was added to the 4-NP solution. At intervals of 3 min, aliquots of the reaction mixture (1.0 mL) were filtered through a 0.2-µm membrane filter, and analyzed via UV-vis spectroscopy at room temperature. According to our previous report [45], the turnover frequency for the 4-NP reduction was obtained from the variations in absorbance at 400 nm.

4. Conclusions

Bimetallic NPs composed of Au and Pd have been successfully synthesized on highly crystalline TOCN via high-densities of carboxylate on the surface in a facile one-pot reaction. AuPdNPs with varying molar ratios of Au and Pd were successfully immobilized and possibly exposed on the TOCN supports. The catalytic activity of AuNPs@TOCN was much higher than the support-free AuNPs and previously reported AuNPs-polymer composites. Furthermore, tailoring the Au and Pd molar ratios had great influence on the catalytic activities for the reduction of 4-NP to 4-AP. In this study a molar ratio of 3:1 (Au:Pd) provided the best catalytic performance. These results suggest that the as-designed TOCN is a promising polymer-type support for metal NP catalysts. The TOCN matrix is easily obtained from a variety of native cellulose sources, and the immobilization of other metal NPs is also possible via a similar strategy. Thus, this novel synthesis approach for the design of hybrid metal NPs@polymer supports, offers great potential for advanced catalytic applications.

Acknowledgments

References

1. Pardo-Yissar, V.; Gabai, R.; Shipway, A.N.; Bourenko, T.; Willner, I. Gold nanoparticle/hydrogel composites with solvent-switchable electronic properties. *Adv. Mater.* **2001**, *13*, 1320–1323.

2. Pastoriza-Santos, I.; Gomez, D.; Perez-Juste, J.; Liz-Marzan, L.M.; Mulvaney P. Optical properties of metal nanoparticle coated silica spheres: A simple effective medium approach. *Phys. Chem. Chem. Phys.* **2004**, *6*, 5056–5060.

3. Yu, C.H.; Al-Saadi, A.; Shih, S.J.; Qiu, L.; Tam, K.Y.; Tsang, S.C. Immobilization of BSA on silica-coated magnetic iron oxide nanoparticle. *J. Phys. Chem. C* **2009**, *113*, 537–543.

4. Narayanan, R.; El-Sayed, M.A. Effect of catalysis on the stability of metallic nanoparticles: Suzuki reaction catalyzed by PVP-palladium nanoparticles. *J. Am. Chem. Soc.* **2003**, *125*, 8340–8347.

5. Haruta, M.; Date, M. Advances in the catalysis of Au nanoparticles. *Appl. Catal. A Gen.* **2001**, *222*, 427–437.

6. Zhu, Y.; Jin, R.; Sun, Y. Atomically monodisperse gold nanoclusters catalysts with precise core-shell structure. *Catalysts* **2011**, *1*, 3–17.

7. Zhen, M.; Sheng, D. Design of novel structured gold nanocatalysts. *ACS Catal.* **2011**, *1*, 805–818.

8. Son, S.U.; Jang, Y.; Park, J.; Na, H.B.; Park, H.M.; Yun, H.J.; Lee, J.; Hyeon, T. Designed synthesis of atom-economical Pd/Ni bimetallic nanoparticle-based catalysts for Sonogashira coupling reactions. *J. Am. Chem. Soc.* **2004**, *126*, 5026–5027.

9. Peng, Z.; Yang, H. Synthesis and oxygen reduction electrocatalytic property of Pt-on-Pd bimetallic heteronanostructures. *J. Am. Chem. Soc.* **2009**, *131*, 7542–7543.

10. Wang, X.; Kariuki, N.; Vaughey, J.T.; Goodpaster, J.; Kumar, R.; Myers, D.J. Bimetallic Pd-Cu oxygen reduction electrocatalysts. *J. Electrochem. Soc.* **2008**, *155*, B602–B609.

11. Hsier, C.T.; Lin, J.Y. Fabrication of bimetallic Pt-M (M = Fe, Co, and Ni) nanoparticle/carbon nanotube electrocatalysts for direct methanol fuel cells. *J. Power Sources* **2009**, *188*, 347–352.

12. Hou, W.; Dehm, N.A.; Scott, R.W.J. Alcohol oxidations in aqueous solutions using Au, Pd, and bimetallic AuPd nanoparticle catalysts. *J. Catal.* **2008**, *253*, 22–27.

13. Liu, J.H.; Wang, A.Q.; Chi, Y.S.; Lin, H.P.; Mou, C.Y. Synergistic effect in an Au-Ag alloy nanocatalyst: CO oxidation. *J. Phys. Chem. B*. **2005**, *109*, 40–43.

14. Jiang, H.L.; Umegaki, T.; Akita, T.; Zhang, X.B.; Haruta, M.; Xu, Q. Bimetallic Au-Ni nanoparticles embedded in SiO_2 nanospheres: Synergetic catalysis in hydrolytic dehydrogenation of ammonia borane. *Chem. Eur. J.* **2010**, *16*, 3132–3137.

15. Fink, J.; Kiely, C.J.; Bethell, D.; Schiffrin, D.J. Self-organization of nanosized gold particles. *Chem. Mater.* **1998**, *10*, 922–926.

16. Harada, G.; Sakurai, H.; Matsushima, M.M.; Izuoka, A.; Sugawara, T. Preparation and characterization of gold nano-particles chemisorbed by π-radical thiols. *Chem. Lett.* **2002**, *31*, 1030–1031.

17. Yokota, S.; Kitaoka, T.; Opietnik, M.; Rosenau, T.; Wariishi, H. Synthesis of gold nanoparticles for in situ conjugation with structural carbohydrates. *Angew. Chem. Int. Ed.* **2008**, *47*, 9866–9869.

18. Grunwaldt, J.D.; Maciejewski, M.; Becker, O.S.; Fabrizioli, P.; Baiker, A. Comparative study of Au/TiO_2 and Au/ZrO_2 catalysts for low-temperature CO oxidation. *J. Catal.* **1999**, *186*, 458–469.

19. Costello, C.K.; Guzman, J.; Yang, J.H.; Wang, Y.M.; Kung, M.C.; Gates, B.C.; Kung, H.H. Activation of Au/γ-Al$_2$O$_3$ catalysts for CO oxidation: Characterization by X-ray absorption near edge structure and temperature programmed reduction. *J. Phys. Chem. B* **2004**, *108*, 12529–12536.

20. Ding, J.H.; Gin, D.L. Catalytic Pd nanoparticles synthesized using a lyotropic liquid crystal polymer template. *Chem. Mater.* **2000**, *12*, 22–24.

21. Liu, H.; Wang, D.; Shang, S.; Song, Z. Synthesis and characterization of Ag-Pd alloy nanoparticles/carboxylated cellulose nanocrystals nanocomposites. *Carbohydr. Polym.* **2011**, *83*, 38–43.

22. Wang, Y.; Wei, G.; Zhang, W.; Jiang, X.; Zheng, P.; Shi, L.; Dong, A. Responsive catalysis of thermoresponsive micelle-supported gold nanoparticles. *J. Mol. Catal. A Chem.* **2007**, *266*, 233–238.

23. Biffis, A.; Cunial, S.; Spontoni, P.; Prati, L. Microgel-stabilized gold nanoclusters: Powerful "quasi-homogeneous" catalysts for the aerobic oxidation of alcohols in water. *J. Catal.* **2007**, *251*, 1–6.

24. Brown, R.M., Jr.; Saxena, I.M.; Kudlicka, K. Cellulose biosynthesis in higher plants. *Trends Plant Sci.* **1996**, *1*, 149–156.

25. Sturcova, A.; Davies, G.R.; Eichhorn, S.J. Elastic modulus and stress-transfer properties of tunicate cellulose whiskers. *Biomacromolecules* **2005**, *6*, 1055–1061.

26. Romling, U. Molecular biology of cellulose production in bacteria. *Res. Microbiol.* **2002**, *153*, 205–212.

27. Chanzy, H. *Cellulose Sources and Exploitation*; Kennedy, J.F., Philips, G.O., William, P.A., Eds.; Ellis Horwood: New York, NY, USA, 1990; pp. 3–12.

28. Sugiyama, J.; Vuong, R.; Chanzy, H. Electron diffraction study on the two crystalline phases occurring in native cellulose from an algal cell wall. *Macromolecules* **1991**, *24*, 4168–4175.

29. Jakob, H.F.; Fratzl, P.; Tschegg, S.E. Size and arrangement of elementary cellulose fibrils in wood cells: A small-angle X-ray scattering study of *Picea abies*. *J. Struct. Biol.* **1994**, *113*, 13–22.

30. Baker, A.A.; Helbert, W.; Sugiyama, J.; Miles, M.J. High-resolution atomic force microscopy of native *Valonia* cellulose I microcrystals. *J. Struct. Biol.* **1997**, *119*, 129–138.

31. Wada, M.; Okano, T.; Sugiyama, J. Synchrotron-radiated X-ray and neutron diffraction study of native cellulose. *Cellulose* **1997**, *4*, 221–232.

32. Saxena, I.M.; Brown, R.M. Cellulose biosynthesis: Current views and evolving concepts. *Ann. Bot.* **2005**, *96*, 9–21.

33. Herrick, F.W.; Casebier, R.L.; Hamilton, J.K.; Sandberg, K.R. Microfibrillated cellulose: Morphology and accessibility. *J. Appl. Polym. Sci. Appl. Polym. Symp.* **1983**, *37*, 797–813.

34. Turbak, A.F.; Snyder, F.W.; Sandberg, K.R. Microfibrillated cellulose, a new cellulose product: Properties, uses, and commercial potential. *J. Appl. Polym. Sci. Appl. Polym. Symp.* **1983**, *37*, 815–827.

35. Araki, J.; Kuga, S. Effect of trace electrolyte on liquid crystal type of cellulose microcrystals. *Langmuir* **2001**, *17*, 4493–4496.

36. Lima, M.M.D.; Borsali, R. Static and dynamic light scattering from polyelectrolyte microcrystal cellulose. *Langmuir* **2002**, *18*, 992–996.

37. Beck-Candanedo, S.; Roman, M.; Gray, D.G. Effect of reaction conditions on the properties and behavior of wood cellulose nanocrystal suspensions. *Biomacromolecules* **2005**, *6*, 1048–1054.

38. Montanari, S.; Roumani, M.; Heux, L.; Vignon, M.R. Topochemistry of carboxylated cellulose nanocrystals resulting from TEMPO-mediated oxidation. *Macromolecules* **2005**, *38*, 1665–1671.

39. Bordel, D.; Putaux, J.L.; Heux, L. Orientation of native cellulose in an electric field. *Langmuir* **2006**, *22*, 4899–4901.

40. Saito, T.; Nishiyama, Y.; Putaux, J.L.; Vignon, M.; Isogai, A. Homogeneous suspensions of individualized microfibrils from TEMPO-catalyzed oxidation of native cellulose. *Biomacromolecules* **2006**, *7*, 1687–1691.

41. Saito, T.; Kimura, S.; Nishiyama, Y.; Isogai, A. Cellulose nanofibers prepared by TEMPO-mediated oxidation of native cellulose. *Biomacromolecules* **2007**, *8*, 2485–2491.

42. Nishino, T.; Takano, K.; Nakamae, K. Elastic modulus of the crystalline regions of cellulose polymorphs. *J. Polym. Sci. Part B Polym. Phys.* **1995**, *33*, 1647–1651.

43. Yano, H.; Sugiyama, J.; Nakagaito, A.N.; Nogi, M.; Matuura, T.; Hikita, M.; Handa, K. Optically transparent composites reinforced with networks of bacterial nanofibers. *Adv. Mater.* **2005**, *17*, 153–155.

44. Saito, T.; Hirota, M.; Tamura, N.; Kimura, S.; Fukuzumi, H.; Heux, L.; Isogai, A. Individualization of nano-sized plant cellulose fibrils by direct surface carboxylation using TEMPO catalyst under neutral conditions. *Biomacromolecules* **2009**, *10*, 1992–1996.

45. Koga, H.; Tokunaga, E.; Hidaka, M.; Umemura, Y.; Saito, T.; Isogai, A.; Kitaoka, T. Topochemical synthesis and catalysis of metal nanoparticles exposed crystalline cellulose nanofibers. *Chem. Commun.* **2010**, *46*, 8567–8569.

46. Mahmoud, K.A.; Male, K.B.; Hrapovic, S.; Luong, J.H.T. Cellulose nanocrystal/gold nanoparticle composite as a matrix for enzyme immobilization. *ACS Appl. Mater. Interfaces* **2009**, *1*, 1383–1386.

47. Burda, C.; Chen, X.; Narayanan, R.; El-Sayed, M.A. Chemistry and properties of nanocrystals of different shapes. *Chem. Rev.* **2005**, *105*, 1025–1102.

48. Scott; R.W.J.; Wilson, O.M.; Oh, S.K.; Kenik, E.A.; Crooks, R.M. Bimetallic palladium-gold dendrimer-encapsulated catalysts. *J. Am. Chem. Soc.* **2004**, *126*, 15583–15591.

49. Anton, R. Nucleation and growth of Pd-Au alloy particles on crystalline graphite at elevated temperatures. *Phys. Rev. B* **2008**, *70*, 245405:1–245405:7.

50. Kuroda, K.; Ishida, T.; Haruta, M. Reduction of 4-nitrophenol to 4-aminophenol over Au nanoparticles deposited on PMMA. *J. Mol. Catal. A Chem.* **2009**, *298*, 7–11.

51. Zhang, M.; Liu, L.; Wu, C.; Fu, G.; Zhao, M.; He, B. Synthesis, characterization and application of well-defined environmentally responsive polymer brushes on the surface of colloid particles. *Polymer* **2007**, *48*, 1989–1997.

52. Liu, W.; Yang, X.; Huang, W. Catalytic properties of carboxylic acid functionalized-polymer microsphere-stabilized gold metallic colloids. *J. Colloid Interface Sci.* **2006**, *304*, 160–165.

53. Chang, Y.C.; Chen, D.H. Catalytic reduction of 4-nitrophenol by magnetically recoverable Au nanocatalyst. *J. Hazard. Mater.* **2009**, *165*, 664–669.

54. Huang, T.; Meng, F.; Qi, L. Facile synthesis and one-dimensional assembly of cyclodextrin-capped gold nanoparticles and their applications in catalysis and surface-enhanced Raman scattering. *J. Phys. Chem. C* **2009**, *113*, 13636–13642.

55. Wunder, S.; Polzer, F.; Lu, Y.; Mei, Y.; Ballauff, M. Kinetic analysis of catalytic reduction of 4-nitrophenol by metallic nanoparticles immobilized in spherical polyelectrolyte brushes. *J. Phys. Chem. C* **2010**, *114*, 8814–8820.
56. Toshima, N.; Yonezawa, T. Bimetallic nanoparticles-novel materials chemical and physical applications. *New J. Chem.* **1998**, *22*, 1179–1201.